journal

J. Am. Ceram. Soc., 93 [9] 2903–2908 (2010)
DOI: 10.1111/j.1551-2916.2010.03810.x

Coexistence of A- and B-Site Vacancy Compensation in La-Doped $Sr_{1-x}Ba_xTiO_3$

Lin Wang and Yoshio Sakka

National Institute for Materials Science, 1-2-1 Sengen, Tsukuba, Ibaraki 305-0047, Japan

Yang Shao and Gianluigi A. Botton

Department of Materials Science and Engineering, McMaster University, Hamilton, Ontario, Canada L8S 4L7

Taras Kolodiazhnyi†

National Institute for Materials Science, 1-1 Namiki, Tsukuba, Ibaraki 305-0044, Japan

$BaTiO_3$ and $SrTiO_3$ perovskites of the $A^{2+}B^{4+}O_3$ type form complete solid solution, Sr_{1-x} Ba_xTiO_3, which can accommodate a substantial amount of donor dopants, for example, La. At high oxygen partial pressure, La dopants in $SrTiO_3$ are compensated by A-site vacancies, whereas in $BaTiO_3$ they are compensated by B-site vacancies. Therefore, donor compensation in the $Sr_{1-x}Ba_xTiO_3$ solid solution should demonstrate a crossover from the A-site vacancies at $x = 0$ to the B-site vacancies at $x = 1$. One may expect, therefore, that at some critical concentration, x_c, the free energy of the $Sr_{1-x}Ba_xTiO_3$ system can become invariant to the vacancy compensation regime. In other words, the system will adopt either A- or B-site vacancies depending on the target chemical composition. Based on the Rietveld refinement of X-ray diffraction patterns and their phase composition analysis as well as scanning electron microscopic and transmission electron microscopic data, we demonstrate that the 28% La-doped $Sr_{1-x}Ba_xTiO_3$ system equilibrated at 1400°C indeed becomes invariant to the vacancy-type compensation at $x_c \approx 0.25$ and can accommodate A- and B-site vacancies at any given ratio. Finally, we propose a microscopic model based on the off-center Ti displacement and the partial covalency of Ti–O bond to explain the distinct difference in the vacancy compensation mechanisms in $BaTiO_3$ and $SrTiO_3$. These findings are important for a further understanding of the thermodynamics of the intrinsic point defects in perovskites as well as for the improvement of electrical performance of the solid oxide fuel cells, ferroelectric, and voltage-tunable ceramics.

I. Introduction

THE ABO_3 perovskites with A = Pb, Sr, Ba and B = Ti and Zr are band gap insulators that have found a variety of commercial applications owing to their excellent ferroelectric and piezoelectric properties. It has been widely recognized that point defects and impurities play an important role in determining the useful properties of these compounds. The point defect chemistry of donor- and acceptor-doped perovskites has been fairly well understood.[1,2] According to the literature, there are two major mechanisms of donor compensation in $ATiO_3$, namely, electronic and cation vacancy type. Electronic compensation of donor ions dominates at low oxygen partial pressure, P_{O_2}. The main focus of this study, however, is cation vacancy compensation of donors that occurs at high P_{O_2}. We further limit our study to the La ion, which owing to its large ionic radii ($r_{La^{3+}} = 1.36$ Å) is an ideal donor that incorporates exclusively at the A site of the above-mentioned perovskites.

Generally, there are two ways to compensate the donor ions in the ABO_3 perovskites at high P_{O_2}, namely by either A-site vacancy, V_A, or B-site vacancy, V_B. Most of the $ATiO_3$ perovskites prefer to form only one type of cation vacancy when it comes to donor compensation. For example, according to Moos *et al.*[1] and Battle *et al.*,[3] La ions in $SrTiO_3$ are compensated by the A-site vacancies at low La concentrations. At very high La concentrations (40–60%), in addition to A-site vacancies, Moos *et al.*[1] detected a small fraction of Ti vacancies. The fraction of Ti vacancies increases with La concentration, reaching 2% in $Sr_{0.106}La_{0.6}TiO_{3.009}$.

$PbTiO_3$ is another perovskite whose piezoelectric and optical properties are improved by doping with La. At low lead partial pressure, a majority of La dopants in $PbTiO_3$ are compensated by the A-site vacancies, similar to La-doped $SrTiO_3$.[4] However, at high lead pressure, $PbTiO_3$ can accommodate a significant amount of the B-site vacancies. According to Hennings,[4] it was possible to prepare a 30% La-doped $PbTiO_3$ at 1330°C with charge compensation realized by equal number of A- and B-site vacancies. An attempt to compensate La by B-site vacancies alone was not successful and resulted in condensation of the liquid PbO phase.[4] Qualitatively, similar results were obtained for La-doped $Pb(ZrTi)O_3$ equilibrated at 1250°C.[5] It was found, however, that increasing the Zr concentration in $Pb(ZrTi)O_3$ at fixed La content reduces the solubility of V_B.[5] Maximum solubility limit of V_B of around 1.7% was found in a single-phase composition of $Pb_{0.784}La_{0.167}(Ti_{0.5}Zr_{0.5})_{0.983}O_3$.

In contrast to other perovskites, donor compensation in $BaTiO_3$ shows a strong preference for the B-site vacancies.[6–9] Makovec *et al.*[9] investigated the defect compensation mechanism of La-substituted $BaTiO_3$. It was found that the single phase La-doped $BaTiO_3$ can be formed only when La is compensated by Ti vacancies. The solubility limit of La_2O_3 in $BaTiO_3$ was found to reach 8.5 mol% at 1400°C corresponding to the chemical formula. $Ba_{0.70}La_{0.30}Ti_{0.925}(V''''_{Ti})_{0.075}O_3$.[9]

Given the identical structure and similar unit cell size, the distinct compensation mechanisms of donor ions in $SrTiO_3$ and $BaTiO_3$ deserve a comprehensive analysis. In this contribution, we explore the La compensation mechanism in $Sr_{1-x}Ba_xTiO_3$ solid solution equilibrated at 1400°C. We found a composition

D. Lopascu—contributing editor

Manuscript No. 27419. Received January 20, 2010; approved March 17, 2010.
This work was supported by Grant-in-Aid for Scientific Research C # 21560025 provided to T. K. by the Japan Society for the Promotion of Science (JSPS). The Canadian Centre for Electron Microscopy is a facility supported by NSERC and McMaster University. G.A.B. is grateful for the NSERC Discovery funding.
†Author to whom correspondence should be addressed. e-mail: kolodiazhnyi.taras@nims.go.jp

range of x where La is predominantly compensated by either V_A or V_B. Remarkably, we have also found a large composition range of x, where the free energy of the system becomes invariant to the type of cation vacancy compensation and the perovskite compound can accommodate both V_A and V_B at any given concentration ratio.

II. Experimental Procedure

In this study, the concentration of La substituted for A site has been fixed at 28%, which is slightly lower than the solubility limit of La in $BaTiO_3$ at 1400°C.[9] Samples were prepared by the conventional solid-state reaction process using dried $SrCO_3$ (99.99%), $BaCO_3$ (99.99%), TiO_2 (99.99%), and La_2O_3 (99.99%). Three types of the target compositions were prepared (Fig. 1) that accommodate (1) A-site vacancies, (2) B-site vacancies, and (3) equal number of A- and B-site vacancies, $[V_A] = [V_B]$, according to the following chemical formulae:

$$(Sr_{1-x}Ba_x)_{1-3y/2}La_yTiO_3 \quad (1)$$

$$(Sr_{1-x}Ba_x)_{1-y}La_yTi_{1-y/4}O_3 \quad (2)$$

$$(Sr_{1-x}Ba_x)_{1-7y/6}La_yTi_{1-y/6}O_3 \quad (3)$$

where $x = 0$, 0.125, 0.25, 0.375, 0.50, 0.75, and 1.0 and $y = 0.28$. The powders were weighed and mixed by ball milling in ethanol for 20 h. Dried mixtures were calcined at 1100°C for 20 h. The calcined powders were remilled and mixed with 10 wt% polyvinyl alcohol and pressed into pellets of 11 mm diameter and 2 mm thickness. The samples were fired at 1400°C for 20 h in air and then quenched to room temperature. Phase composition was analyzed by powder X-ray diffraction (RINT 2500, Rigaku, Tokyo, Japan) using Cu$K\alpha$ radiation. X-ray diffraction patterns were collected with a step size of 0.02° over the 2Θ angle range of 5–100°. Rietveld refinement of the X-ray data was performed using the RIETAN-2000 software (developed by F. Izumi and T. Ikeda, NIMS, Tsukuba, Japan).[10] Microstructure of polished samples was analyzed using a scanning electron microscope (SEM, JSM6500, Hitachi, Tokyo, Japan). Samples for transmission electron microscopy (TEM) analysis were prepared by the conventional method of manually grinding on SiC paper down to 100 μm thickness, then further dimpling to 20 μm, and finally ion beam thinned until a hole is formed. The high angular annular dark-field imaging and EDS elemental mapping were performed using an FEI Titan 80-300 transmission electron microscope (FEI, Eindhoven, the Netherlands) at the Canadian Center for Electron Microscopy.

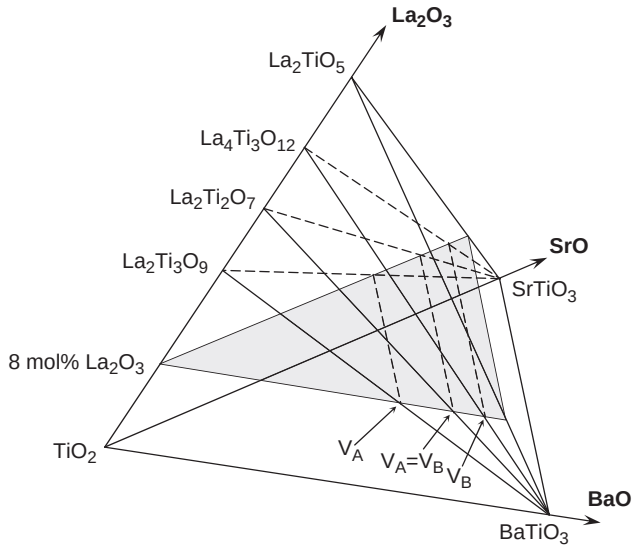

Fig. 1. Schematic representation of the part of the La_2O_3–TiO_2–BaO–SrO quaternary-phase diagram. The target sample compositions are located on the shaded plane at ca. 8 mol% La_2O_3. The compositions are adjusted according to the V_A, V_B, and $[V_A] = [V_B]$ compensation mechanisms indicated by the dashed lines.

III. Results and Discussion

The starting composition, the target vacancy compensation mechanism, and the phases detected after equilibration at 1400°C are summarized in Table I. For convenience, the samples have been labeled according to their Ba concentration, $x \times 100$, and the type of vacancy compensation. For example, sample 50A has $x = 0.5$ and has been compensated by V_A.

Analysis of the lattice parameters (Fig. 2) extracted from the Reitveld refinement provides a general picture of the vacancy compensation regimes in the La-doped $Sr_{1-x}Ba_xTiO_3$ solid solution. As revealed in Fig. 2, for V_A compensation regime, the Vegard's law is satisfied in the $0 \le x \le 0.375$ range; for the V_B compensation, the Vegard's law is obeyed in a much wider concentration range of $0.25 \le x \le 1.0$. As further revealed by the accurate analysis of the X-ray data, for the intermediate values of x, e.g. $0.125 \le x \le 0.5$, there exists a composition field of the $Sr_{1-x}Ba_xTiO_3$ solid solution that can accommodate significant concentrations of both A- and B-site vacancies.

The single-phase compounds of the Sr-end members of the $Sr_{1-x}Ba_xTiO_3$ solid solution form along the $SrTiO_3$–$La_2Ti_3O_9$ tie line according to chemical formula $Sr_{1-3y/2}La_yTiO_3$, which indicates that La ions are predominantly compensated by the V_A defects. These findings are in very good agreement with the literature data on La-doped $SrTiO_3$.[1,3] An attempt to shift the equilibrium toward the V_{Ti} compensation at $x \le 0.125$ (Table I, samples 0AB, 0B) has resulted in the precipitation of the secondary-phase isomorphous with $SrLa_4Ti_4O_{15}$ (ICDD PDF 049-0254). Traces of the $SrLa_4Ti_4O_{15}$-type phase have also been detected in the 12.5B compound (Fig. 4). Appearance of the $SrLa_4Ti_4O_{15}$ phase in the compounds 0B, 0AB, and 12.5B with the target V_B compensation is at variance with the literature data[1] that postulates the formation of the $SrO \cdot nSrTiO_3$ Ruddlesden–Popper secondary phases. For $n \ge 4$, these phases are indistinguishable from the $SrTiO_3$ X-ray pattern.[1] At the moment, we cannot explain this difference, yet our data indicate an existence of the tie line connecting the perovskite $Sr_{1-3y/2}La_yTiO_3$ solid solution with the $SrLa_4Ti_4O_{15}$ ternary phase rather than with the binary $SrO \cdot nSrTiO_3$ Ruddlesden–Popper phases.

One may notice (Fig. 2) that the perovskite lattice parameters of the multiphase 0AB and 0B compounds do not merge with the single-phase sample, 0A, and are somewhat larger. Also, we found that the diffraction peak profiles of the main perovskite phases in the 0AB, 0B, and 12.5B samples are significantly broadened. All this evidence suggests that there exists a strong interaction between the perovskite phase and the $SrLa_4Ti_4O_{15}$ secondary phase detected in these samples. Namely, we speculate that the $SrLa_4Ti_4O_{15}$ phase may intergrow within the perovskite lattice generating a tensile lattice strain that would expand the unit cell of the perovskite phase. TEM analysis of the 12.5B sample has fully confirmed the above hypothesis.

Top panel of Fig. 3 is a high-angle annular dark-field STEM image of a representative area of sample 12.5B that shows a plate-like secondary phase intergrown into the main matrix grain. The secondary phase appears bright on the image, which indicates that it contains a higher concentration of heavy atoms as compared with the main perovskite phase. EDS elemental mapping of Sr and La atoms shown at the bottom panel of Fig. 3 confirms that the secondary phase is enriched with La atoms and deficient of Sr. This observation stands in excellent agreement with the XRD analysis that reveals traces of the $SrLa_4Ti_4O_{15}$ secondary phase in the 12.5B sample.

The $SrLa_4Ti_4O_{15}$ phase is isomorphous with the trigonal $Ba_5Ta_4O_{15}$ and $Ba_5Nb_4O_{15}$ compounds. It can be treated as a

Table I. Target Compositions, Target Compensation Mechanism of La-Donors, and Resulted Phases After Equilibration in Air at 1400°C

Sample	Target formula	Compensation of La	Compounds detected
0A	$Sr_{0.58}La_{0.28}TiO_3$	$[V_A]$	P_{ss}
0AB	$Sr_{0.673}La_{0.28}Ti_{0.953}O_3$	$[V_A] = [V_B]$	P_{ss}, SL_2T_4
0B	$Sr_{0.72}La_{0.28}Ti_{0.93}O_3$	$[V_B]$	P_{ss}, SL_2T_4
12.5A	$(Sr_{0.875}Ba_{0.125})_{0.58}La_{0.28}TiO_3$	$[V_A]$	P_{ss}
12.5AB	$(Sr_{0.875}Ba_{0.125})_{0.673}La_{0.28}Ti_{0.953}O_3$	$[V_A] = [V_B]$	P_{ss}
12.5B	$(Sr_{0.875}Ba_{0.125})_{0.72}La_{0.28}Ti_{0.93}O_3$	$[V_B]$	P_{ss}, $(SB)L_2T_4$
25A	$(Sr_{0.75}Ba_{0.25})_{0.58}La_{0.28}TiO_3$	$[V_A]$	P_{ss}
25AB	$(Sr_{0.75}Ba_{0.25})_{0.673}La_{0.28}Ti_{0.953}O_3$	$[V_A] = [V_B]$	P_{ss}
25B	$(Sr_{0.75}Ba_{0.25})_{0.673}La_{0.28}Ti_{0.953}O_3$	$[V_B]$	P_{ss}
37.5A	$(Sr_{0.625}Ba_{0.375})_{0.58}La_{0.28}TiO_3$	$[V_A]$	P_{ss}, $(SB)T_4$, $(SB)LT_{4ss}$
37.5AB	$(Sr_{0.625}Ba_{0.375})_{0.673}La_{0.28}Ti_{0.953}O_3$	$[V_A] = [V_B]$	P_{ss}
37.5B	$(Sr_{0.625}Ba_{0.375})_{0.72}La_{0.28}Ti_{0.93}O_3$	$[V_B]$	P_{ss}
50A	$(Sr_{0.5}Ba_{0.5})_{0.58}La_{0.28}TiO_3$	$[V_A]$	P_{ss}, $(SB)T_4$, $(SB)LT_{4ss}$
50-2AB	$(Sr_{0.5}Ba_{0.5})_{0.65}La_{0.28}Ti_{0.965}O_3$	$2[V_A] = [V_B]$	P_{ss}
50AB	$(Sr_{0.5}Ba_{0.5})_{0.673}La_{0.28}Ti_{0.953}O_3$	$[V_A] = [V_B]$	P_{ss}
50B	$(Sr_{0.5}Ba_{0.5})_{0.72}La_{0.28}Ti_{0.93}O_3$	$[V_B]$	P_{ss}
75A	$(Sr_{0.25}Ba_{0.75})_{0.58}La_{0.28}TiO_3$	$[V_A]$	P_{ss}, $(SB)T_4$, $(SB)LT_{4ss}$
75AB	$(Sr_{0.25}Ba_{0.75})_{0.673}La_{0.28}Ti_{0.953}O_3$	$[V_A] = [V_B]$	P_{ss}, $(SB)LT_{3ss}$, $(SB)LT_{4ss}$
75A2B	$(Sr_{0.25}Ba_{0.75})_{0.692}La_{0.28}Ti_{0.944}O_3$	$[V_A] = 2[V_B]$	P_{ss}, $(SB)LT_{3ss}$, $(SB)_2L_2T_5$
75B	$(Sr_{0.25}Ba_{0.75})_{0.72}La_{0.28}Ti_{0.93}O_3$	$[V_B]$	P_{ss}
100A	$Ba_{0.58}La_{0.28}TiO_3$	$[V_A]$	P_{ss}, BT_4, BLT_{4ss}
100AB	$Ba_{0.673}La_{0.28}Ti_{0.953}O_3$	$[V_A] = [V_B]$	P_{ss}, BLT_3, BLT_{4ss}
100B	$Ba_{0.72}La_{0.28}Ti_{0.93}O_3$	$[V_B]$	P_{ss}

P_{ss}, La-doped $Sr_{1-x}Ba_xTiO_3$ perovskite solid solution; SL_2T_4, $SrLa_4Ti_4O_{15}$; $(SB)L_2T_4$, $(Sr,Ba)La_4Ti_4O_{15}$; SBT_4, $(Sr,Ba)Ti_4O_9$; $SBLT_3$, $(Sr,Ba)La_2Ti_3O_{10}$; $(SB)_2L_2T_5$, $(Sr,Ba)_2La_4Ti_5O_{18}$; $(SB)LT_{4ss}$, $(SrBa)La_2Ti_4O_{12}$; and BT_4, $BaTi_4O_9$.

perovskite viewed along the cubic body diagonal, which shows a repetition of an A B C A B sequence of the $5(Sr,La)O_3$ layers. Ti ions are located inside the corner-sharing oxygen octahedra. This repetition is interrupted after each $5(Sr,La)O_3$ layers by the two face-sharing oxygen octahedra accommodating Ti vacancies. The trigonal cell parameters of the $SrLa_4Ti_4O_{15}$ are $a = 5.55$ Å and $c = 11.066$ Å. Therefore, the (100) lattice planes of the $SrLa_4Ti_4O_{15}$ provide a natural template for the growth of the La-doped $(SrBa)TiO_3$ perovskite along the cubic (111)

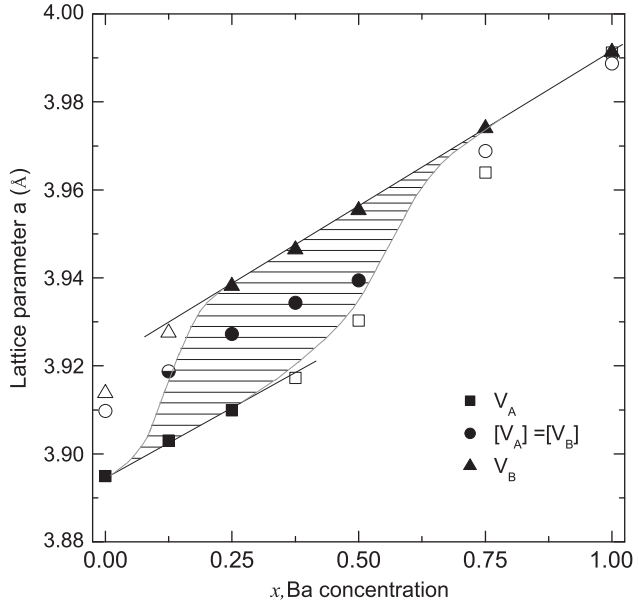

Fig. 2. Ba concentration dependence of the lattice parameter of 28 at.% La-doped $Sr_{1-x}Ba_xTiO_3$ solid solution prepared according to different vacancy compensation mechanisms. Squares, triangles, and circles correspond to V_A, V_B, and $[V_A] = [V_B]$ compensation, respectively. Solid symbols correspond to single-phase perovskite compositions, whereas open symbols represent multiphase compounds. Hatched area indicates a single-phase composition field where a given fraction of V_A and V_B vacancies coexists. Lattice constant of sample 12.5AB is marked by a half-filled circle because its X-ray diffraction pattern shows some weak and broad peak at $2\Theta = 28°$ that may be attributed to small traces of amorphous phase.

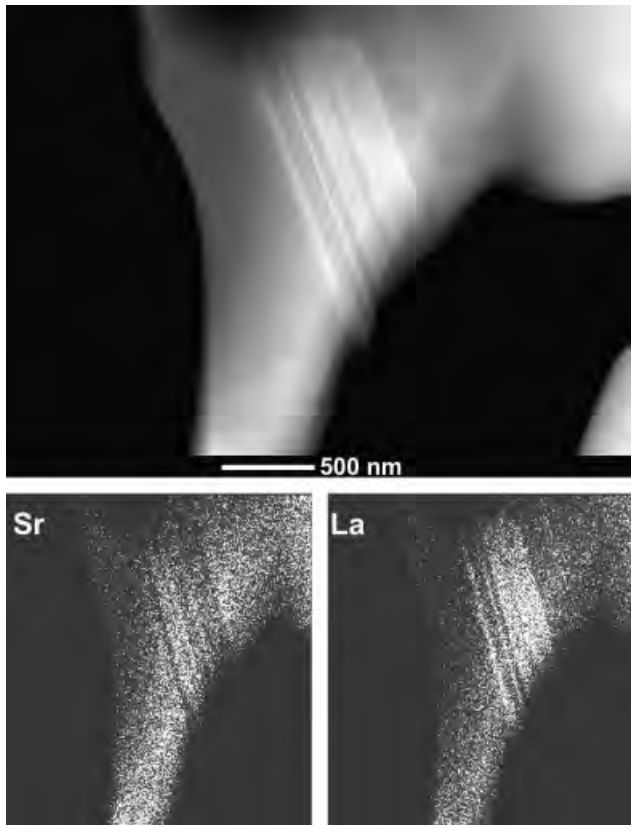

Fig. 3. *Top panel*: The high-angular annular dark-field STEM micrograph of sample 12.5B. $(Sr,Ba)La_4Ti_4O_{15}$ secondary phase intergrown into the matrix phase appears brighter as it contains higher concentration of heavy (La) atoms. *Bottom panel*: EDS maps of Sr and La atoms, which confirm that the secondary phase is La rich and Sr deficient.

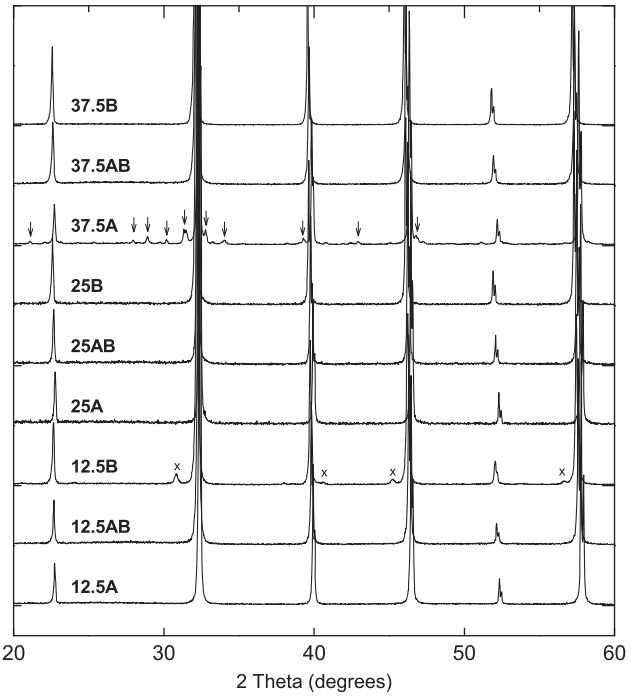

Fig. 4. X-ray diffraction patterns of selected compounds. Note that the samples 25A, 25AB, and 25B are single phase. Arrows indicate $BaTi_4O_9$- and $BaLa_2Ti_4O_{12}$-type secondary phases in the 37.5A sample. Extra reflections marked by x in the 12.5B compound indicate $SrLa_4Ti_4O_{15}$-type secondary phase.

direction. The lattice constant of the Sr-end member of our perovskite series with A-site compensation, 0A, $a_p = 3.8950(5)$ Å (Fig. 2). This translates into $a_p\sqrt{2} = 5.50836$Å, which is $\approx 1\%$ smaller than the trigonal cell parameter a of the $SrLa_4Ti_4O_{15}$. The tensile lattice strain developed in the main perovskite phase is responsible for the apparent increase in the lattice parameters of the 0AB, 0B, and 12.5B samples containing $(Sr,Ba)La_4Ti_4O_{15}$ secondary phase (Fig. 2).

On the Ba-rich side, La compensation is accommodated by V_{Ti}. In fact, predominant V_{Ti} compensation holds for $0.75 \leq x \leq 1$. In this range of x, single-phase compositions form along the $(Ba,Sr)TiO_3$–$La_4Ti_3O_{12}$ tie line (Table I, samples 100B, 75B). An attempt to introduce a small concentration of V_A defects in sample 75A2B results in the precipitation of the secondary phases isomorphous with $BaLa_2Ti_3O_{10}$ (ICDD PDF 042-0418) and $Ba_2La_4Ti_5O_{18}$ (ICDD PDF 049-1013). Further shift toward V_A compensation targeted in sample 75AB leads to the formation of the $BaLa_2Ti_4O_{12}$-type phase (ICDD PDF 045-0117) and the disappearance of the $Ba_2La_4Ti_5O_{18}$-type phase. Finally, an only V_A compensation targeted in sample 75A results in the formation of the $BaTi_4O_9$- and $BaLa_2Ti_4O_{12}$-type secondary phases. These findings indicate that for $0.75 \leq x \leq 1$, the La_2O_3–$(Sr_{1-x}Ba_x)O$–TiO_2 pseudoternary phase diagram is identical to that of the La_2O_3–BaO–TiO_2 ternary in the composition region close to the La-doped $BaTiO_3$ perovskite solid solution.[9]

In contrast to the original assumption[11] that La donors are compensated by A-site vacancies in $BaTiO_3$, our results confirm once again that excess positive charge of La ions is compensated by B-site vacancies in $BaTiO_3$ as well as in the $Sr_{1-x}Ba_xTiO_3$ solid solution for $0.75 \leq x \leq 1$. On the Sr-rich side of the $Sr_{1-x}Ba_xTiO_3$ solid solution, A-site vacancies are predominant compensation defects for $x < 0.125$. Furthermore, analysis of the single-phase composition region as well as magnetic susceptibility[‡] indicates that A- and B-site vacancies in highly La-doped $Sr_{1-x}Ba_xTiO_3$ solid solution are completely ionized, namely, they exist in the form of V_A'' and V_{Ti}'''' where each A- and B-site vacancy compensate two and four La ions, respectively. These findings are in excellent agreement with recent first-principles calculations of energetics of the A- and B-site vacancies in $BaTiO_3$.[12] We emphasize, however, that our results do not rule out the existence of a small concentration of partially ionized A- or B-site vacancies in lightly donor-doped ceramics, especially in the PTC-thermistor ceramics with partial electronic compensation.[13]

During the course of this work, we found a critical concentration of Ba at $x_c \approx 0.25$ where both A- and B-site vacancies can be accommodated in the perovskite lattice depending on the targeted vacancy compensation regime, e.g., V_A or V_B. At this Ba concentration, the chemical potential of the B-site vacancy is equal to that of the A-site vacancy and the free energy of the system becomes invariant to the type of cation vacancy compensation. The system can easily accommodate both A- and B-site vacancies at any given ratio (Fig. 4, samples 25A, 25AB, and 25B, and also Figs. 5(a)–(c)). Analysis of the data allows us to determine the single-phase composition field within the part of the La_2O_3–TiO_2–BaO–SrO quaternary-phase diagram dissected at ca. 8 mol% La_2O_3 (Fig. 6). These findings open up several exciting opportunities for further research. For example, one can now separate the effect of the V_A and V_B contributions to the voltage tunability, dielectric loss, leakage currents, and ferroelectric aging of the $Sr_{1-x}Ba_xTiO_3$-based perovskites. Another opportunity comes from the field of the solid oxide fuel cells (SOFC) where A- and B-site vacancy compensation can modify the electron and ion transport as well as catalytic activity of the La- and Nb-doped $SrTiO_3$-based SOFC anodes.[14,15]

Finally, we would like to address the possible reasons for the two distinct vacancy compensation mechanisms in $SrTiO_3$ and $BaTiO_3$. From the first glance, one may think of V_{Ti}'''' as the most unlikely defect in $ATiO_3$ perovskite. Because of its high effective charge, this defect would cause a major perturbation to the crystal field due to the close proximity to the six surrounding oxygens located at a distance of half a unit cell, $a/2$. Therefore, the total energy cost to accommodate this defect in the ideal perovskite lattice is very high. This is why it does not form in $SrTiO_3$, where donors are compensated by V_A'' surrounded by 12 neighbor oxygens at a distance of $a/\sqrt{2}$.

Why then in $BaTiO_3$ donor dopants are compensated by the V_{Ti}'''' instead of V_A''? The short answer to this question is that $BaTiO_3$ is not an "ideal" perovskite. As revealed by detailed diffraction,[16] NMR,[17] and EXAFS[18] studies, Ti ions in $BaTiO_3$ are displaced from the center of the oxygen octahedra along one of the $\langle 111 \rangle$ directions by a distance of ≈ 0.1–0.14 Å. In pure $BaTiO_3$, this displacement brings a strong O–Ti hybridization that drives ferroelectric instability.[19] Recent studies on the local symmetry of Ti ions using the pair distribution function analysis have revealed that Ti remains off-center in $BaTiO_3$ doped with a high concentration of donor ions, albeit on a macroscopic scale, the structure appears cubic.[20] We argue that the off-center Ti position and its ability to form a partially covalent bond with neighbor oxygens are the main factors that minimize the energy of the titanium vacancies in donor-doped $BaTiO_3$. The large negative charge of Ti vacancy in $BaTiO_3$ is compensated by the lattice relaxation around this defect, and more importantly by the transfer of the excess negative charge from the V_{Ti}''''-adjacent oxygens to the neighbor Ti ions owing to the partially covalent Ti $3d$–O $2p$ bonding.

This rationale can be extended further to explain why La-doped $PbTiO_3$ can also accommodate significant amount of Ti vacancies.[4] It is known that in $PbTiO_3$, in addition to the partially covalent Ti–O bond, there exists a strong hybridization between lead $6s$ and oxygen $2p$ states, which is responsible for the anomalously strong tetragonal distortion of the $PbTiO_3$ ground state.[19] Therefore, the ability of oxygens to transfer part of the negative charge back to Pb ions can reduce the overall effective charge of the V_{Ti}'''' defect and make it energetically more stable.

‡Magnetic susceptibility of highly La-doped $Sr_{1-x}Ba_xTiO_3$ shows diamagnetic response that remains temperature independent in the 30–300 K range. We found no evidence of substantial concentration of paramagnetic centers that can be attributed to partially ionized V_A or V_B vacancies with unpaired electron spin. Detailed analysis of magnetic data will be presented elsewhere.

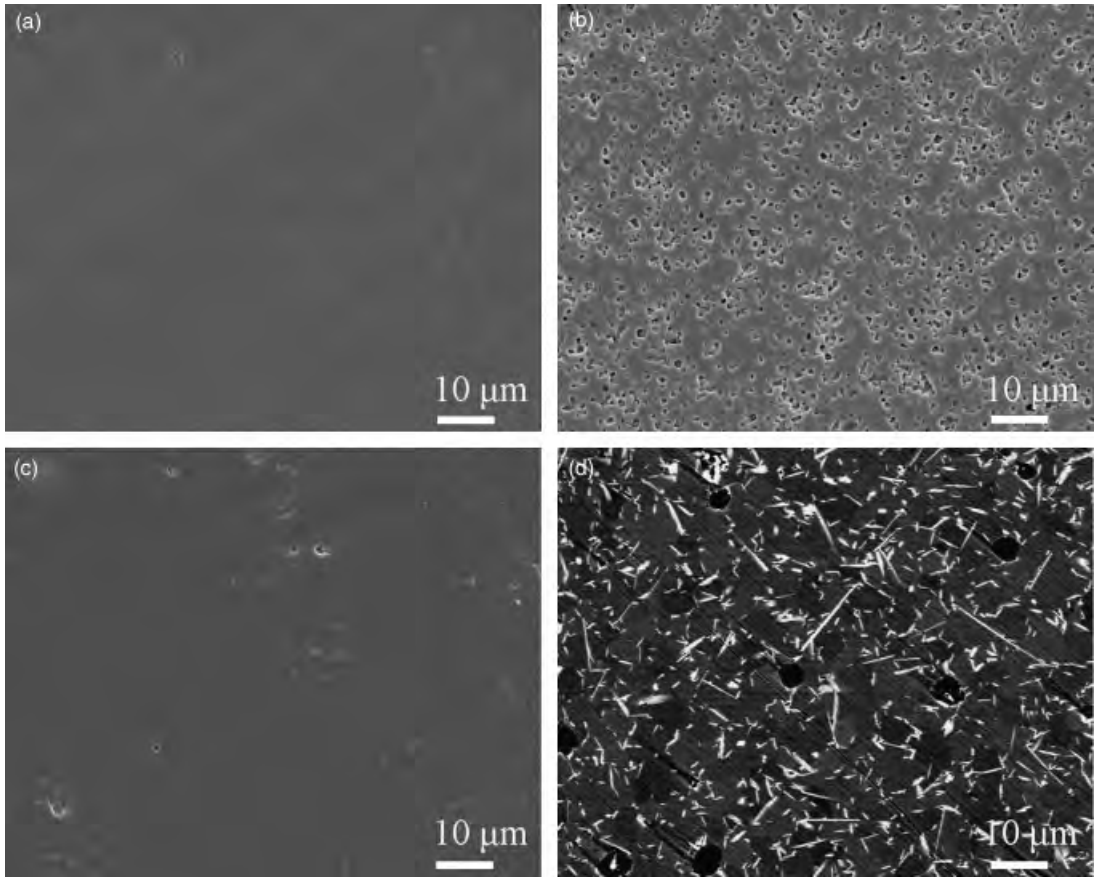

Fig. 5. The scanning electron micrographs (SEM) of samples (a) 25A, (b) 25AB, (c) 25B, and (d) 37.5A. According to the SEM and X-ray diffraction data, samples 25A, 25B, and 25 AB are single-phase perovskites. Sample 37.5A, in addition to the main perovskite phase, contains two types of secondary phases: $(Sr,Ba)Ti_4O_9$ and light-gray needle-like $(SrBa)La_2Ti_4O_{12}$.

In conclusion, we have investigated the part of the La_2O_3–TiO_2–BaO–SrO quaternary-phase diagram in the composition range close to the $Sr_{1-x}Ba_xTiO_3$ perovskite solid solution doped with 28% La on the A site. We have determined the composition region where La donors are compensated by A- and/or B-site vacancies. Furthermore, we found a composition field where large concentrations of A- and B-site vacancies can coexist in the system. Finally, it was found that at $x \approx 0.25$, the system becomes completely invariant to the type of the vacancy compensation. While the BaO-rich part of the La_2O_3–TiO_2–BaO–SrO quaternary-phase diagram is consistent with the literature data,[9] our results on the SrO-rich part are in some disagreement with earlier reports.[1] In particular, based on the XRD, Rietveld refinement, and TEM data, we suggest that there exists a tie line connecting the perovskite $Sr_{1-3y/2}La_yTiO_3$ solid solution with the $SrLa_4Ti_4O_{15}$ ternary phase. Finally, we suggest that the difference in the vacancy compensation mechanism in $SrTiO_3$ and $BaTiO_3$ has a microscopic origin, namely, we propose that significant off-center displacement of Ti ion and hybridization of the Ti 3*d* and O 2*p* electronic states can partially compensate for the large negative charge of the V_{Ti}'''' defect in $BaTiO_3$, whereas in the $SrTiO_3$ this possibility is limited by the highly symmetric Ti position in the center of the oxygen octahedra.

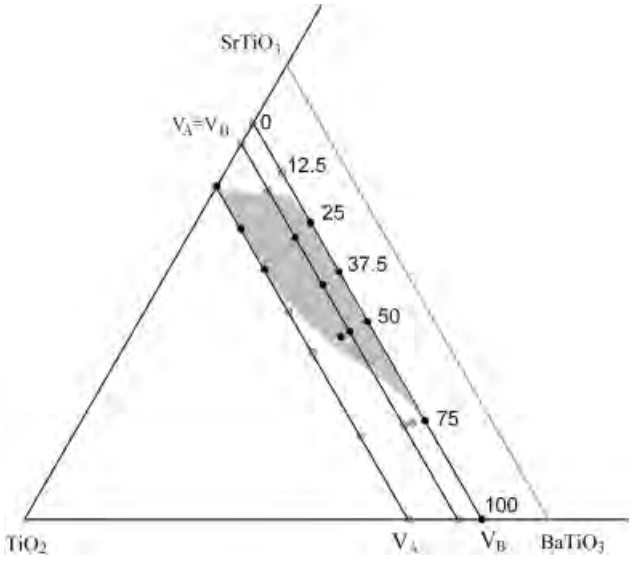

Fig. 6. Projection of the part of the La_2O_3–TiO_2–BaO–SrO quaternary-phase diagram dissected at ca. 8 mol% La_2O_3. The gray dots represent multiphase compounds. Black dots are single-phase perovskite solid solution of $Sr_{1-x}Ba_xTiO_3$ doped with 28% La on the A site. The gray area indicates the single-phase composition range. The numbers correspond to $x \times 100$. V_A, V_B, and $[V_A] = [V_B]$ denote different vacancy compensation mechanisms. To determine the boundary of the single-phase region more accurately, we have added two more compositions: 50-2AB and 75A2B with $2[V_A] = [V_B]$ and $[V_A] = 2[V_B]$ compensation, respectively (Table I).

References

[1]R. Moos, T. Bischoff, W. Menesklou, and K. H. Härdtl, "Solubility of Lanthanum in Strontium Titanate in Oxygen-Rich Atmosphere," *J. Mater. Sci.*, **32**, 4247–52 (1997).

[2]U. Balachandran and N. G. Eror, "Solubility of Lanthanum in Strontium Titanate," *J. Am. Ceram. Soc.*, **64**, c-75–6 (1981).

[3]P. D. Battle, J. E. Bennett, J. Sloan, R. J. D. Tilley, and J. F. Vente, "A-Site Cation-Vacancy Ordering in $Sr_{1-3x/2}La_xTiO_3$: A Study by HRTEM," *J. Solid State Chem.*, **149**, 360–96 (2000).

[4]D. Hennings, "The Range of Existence of Perovskite Phases in the System PbO–TiO_2–La_2O_3," *Mat. Res. Bull.*, **6**, 329–40 (1971).

[5]K. H. Härdtl and D. Hennings, "Distribution of A-Site and B-Site Vacancies in (Pb,La)(Ti,Zr)O_3 Ceramics," *J. Am. Ceram. Soc.*, **55**, 230–1 (1971).

[6]G. H. Jonker and E. E. Havinga, "The Influence of Foreign Ions on the Crystal Lattice of Barium Titanate," *Mat. Res. Bull.*, **17**, 345–50 (1982).

[7]H. M. Chan, M. P. Harmer, and D. M. Smyth, "Compensating Defects in Highly Donor-Doped $BaTiO_3$," *J. Am. Ceram. Soc.*, **69**, 507–710 (1986).

[8]J. M. Millet, R. S. Roth, L. T. Ettlinger, and H. S. Parker, "Phase Equilibria and Crystal Chemistry in the Ternary System BaO–TiO_2–Nb_2O_5," *J. Solid State Chem.*, **67**, 259–70 (1987).

[9]D. Makovec, Z. Samardzija, U. Delalut, and D. Kolar, "Defect Structure and Phase Relations of Highly Lanthanum-Doped Barium Titanate," *J. Am. Ceram. Soc.*, **78**, 2193–7 (1995).

[10]F. Izumi and T. Ikeda, "A Rietveld-Analysis Program RIETAN-98 and Its Applications to Zeolites," *Mater. Sci. Forum*, **321**, 198–205 (2000).

[11]J. Daniels and K. H. Härdtl, "Part I, Electrical Conductivity at High Temperatures of Donor-Doped Barium Titanate Ceramics," *Phillips Res. Repts.*, **31**, 487–559 (1976).

[12]P. Erhart and K. Albe, "Thermodynamics of Mono- and Di-Vacancies in Barium Titanate," *J. Appl. Phys.*, **102**, 084111, 8pp (2007).

[13]T. Kolodiazhnyi and A. Petric, "Analysis of Point Defects in Polycrystalline $BaTiO_3$ by Electron Paramagnetic Resonance," *J. Phys. Chem. Solids*, **64**, 953–60 (2003).

[14]C. D. Savaniu and J. T. S. Irvine, "Reduction Studies and Evaluation of Surface Modified A-Site Deficient La-Doped $SrTiO_3$ as Anode Material for IT-SOFCs," *J. Mater. Chem.*, **19**, 8119–29 (2009).

[15]P. Blennow, K. K. Hansen, L. R. Wallenberg, and M. Mogensen, "Electrochemical Characterization and Redox Behavior of Nb-Doped $SrTiO_3$," *Solid State Ionics*, **180**, 63–70 (2009).

[16]R. Comes, M. Lambert, and A. Guinier, "The Chain Structure of $BaTiO_3$ and $KNbO_3$," *Solid State Commun.*, **6**, 715–9 (1968).

[17]B. Zalar, A. Lebar, J. Seliger, R. Blinc, V. V. Laguta, and M. Itoh, "NMR Study of Disorder in $BaTiO_3$ and $SrTiO_3$," *Phys. Rev. B*, **71**, 064107, 12pp (2005).

[18]E. A. Stern, "Character of Order–Disorder and Displacive Components in Barium Titanate," *Phys. Rev. Lett.*, **93**, 037601, 3pp (2004).

[19]R. E. Cohen, "Origin of Ferroelectricity in Perovskite Oxides," *Nature*, **358**, 136–8 (1992).

[20]K. Page, T. Kolodiazhnyi, T. Proffen, A. K. Cheetham, and R. Seshadri, "Local Structural Origins of the Distinct Electronic Properties of Nb-Substituted $SrTiO_3$ and $BaTiO_3$," *Phys. Rev. Lett.*, **101**, 205502, 4pp (2008). □